Effect of growth orientation and surface roughness on electron transport in silicon nanowires

Alexei Svizhenko,* Paul W. Leu,† and Kyeongjae Cho‡
Department of Mechanical Engineering, Stanford University, Stanford, California 94305, USA

(Received 7 October 2006; published 14 March 2007)

We report a study of the effect of growth orientation and surface roughness on electron transport in small-diameter hydrogen passivated silicon nanowires (NWs). We employ a nonequilibrium Green's function technique within an $sp^3d^5s^*$ tight-binding approximation to show that band structure strongly affects current-voltage characteristics of ideal NWs, leading to current falloff at high drain bias for certain growth orientations. Surface roughness suppresses small bias conductance and current, and leads to a nonmonotonic dependence on gate bias. We also find that surface roughness results in a decrease of current with the length of a NW. The rate of the decrease depends on the growth directions and diameter. As the diameter of a NW becomes smaller, a transition of electron transport to Anderson localization regime may occur even at room temperature.

DOI: 10.1103/PhysRevB.75.125417 PACS number(s): 73.63.Nm, 84.71.Mn

I. INTRODUCTION

Silicon nanowires (Si NWs) are a promising nanomaterial for nanoscale interconnects and nanodevice applications (e.g., nanotransistors). Many experimental groups have fabricated NWs and measured their current-voltage (*I-V*) curves by attaching metal electrodes at both ends of NWs.[1–6] The measured *I-V* curves have shown diverse conductance behaviors depending on the NW surface conditions and other external effects. Even though some measurements indicate a possibility of very high mobility and high sensitivity to chemical modification of NW surfaces, the detailed mechanisms of electron transport in the presence of external factors (e.g., surface roughness, surface defects, and dopants) are not well understood yet.

Most of the fabricated NWs reported up to date had diameters of 10–100 nm. However, in order to compete with planar complementary metal-oxide-semiconductor technology below 10 nm gate length, the diameter of NWs used as channels of novel field-effect transistors should be reduced down to 1–5 nm. Such a small diameter is required to minimize short channel effects and to establish a good electrostatic control by the gate over the channel. Recent experiments demonstrated that fabrication of small-diameter (1–2 nm) NWs is possible.[1] It was also shown theoretically that [110] NWs with hexagonal cross section can be energetically stable at diameters of 1.2 nm and above[7] and thus experimentally achievable. Current fabrication methods of Si NWs such as vapor-liquid-solid (VLS) method assisted by a catalyst particle usually involve a vertical NW growth with the catalyst particle on the top end of the wire. Fluctuations of the particle diameter during the growth process lead to the variations of diameter of the NW from layer to layer. Numerous high-resolution transmission electron microscopy images of NWs available in the literature reveal that the surface of fabricated NWs is always ridden by one to two monolayer steps, which suggests that the surface roughness is inherent to the fabrication method. Periodic sawtooth faceting has also been observed in Si NWs.[8]

Theoretical studies of NWs so far have been limited to studying the effects of ideal structure,[9] surface,[10] low drain bias conductance,[11] defects,[12] and morphology and doping[13] on electronic properties of ideal NWs. Reference 14 addressed the effects of surface roughness on the performance of Si NW transistors using the effective-mass approximation and concluded that the effect of surface roughness in small-diameter wires with fewer modes is less than in bulk transistors where many modes are occupied. Related to effects of surface roughness in one-dimensional systems is a theoretical[15] and experimental[16] study of influence of point defects on the ballistic electron transport in carbon nanotubes (CNTs). These studies reported an exponential decrease of low-bias conductance with the length of CNT due to the presence of point defects and a transition to Anderson localization regime. To the best of our knowledge, the atomistic theoretical study of the effects of surface roughness in Si NW has not been performed.

In this paper, we study the effect of growth orientation and surface roughness on the current-voltage characteristics of small-diameter Si NWs using atomistic calculations. In Sec. II, we describe the method and assumptions of the model we use. We then discuss in Sec. III A the current-voltage characteristics of ideal NWs of different growth directions. Sec. III B deals with the effects of surface roughness on conducting properties of NWs. We conclude in Sec. IV.

II. METHOD

The basic structures in our study are small-diameter (0.46–1.56 nm) Si NWs grown in [110], [100], and [111] directions, whose cross sections are shown in Fig. 1. All

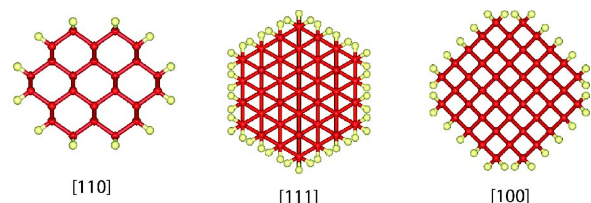

FIG. 1. (Color online) Cross sections of silicon nanowires grown in [110], [111], and [100] directions passivated with hydrogen atoms. The diameters are 1.26, 1.52, and 1.56 nm, respectively.

 ©2007 The American Physical Society

wires are passivated with hydrogen atoms so that there are no surface states. The Si-Si and Si-H bonds have lengths of 2.37 and 1.48 Å respectively, obtained from *ab initio* density-functional theory with generalized gradient approximation (DFT-GGA) using Vienna ab-initio simulation package (VASP).[17] The wire cross sections are cut using the low free energy (110), (100), and (111) facets, consistent with what has been suggested experimentally and theoretically.[1,7]

Having obtained the atomic structure, we conducted non-equilibrium Green's function (NEGF) calculations of electron transport within a tight-binding approximation. A ten orbital $sp^3d^5s^*$ tight-binding Hamiltonian was constructed using a scheme described in Ref. 18 with coupling parameters between Si and H atoms taken from Ref. 11. Thus, the change of the three-dimensional geometry of the structure due to surface roughness is fully taken into account in the Hamiltonian. We checked to confirm that the tight-binding model employed reproduces all the key features of NW band structure and is in good agreement with *ab initio* DFT-GGA calculations. In our calculations, the length of nanowires was ~390 nm with a total of ~40 000–50 000 atoms. Due to the large size of the system, the tight-binding approximation has a computational advantage over a local basis DFT approach. The advantage comes mainly from the approximation of the nearest-neighbor interaction.

The calculation of transmission, current, and local density of states (DOS) was done by using a recursive Green's function algorithm, described in, e.g., Refs. 19 and 20. A nanowire was divided into layers corresponding to atomic planes, perpendicular to the axis of the wire. Due to the nearest-neighbor interaction, each layer would consist of just one atomic plane. Thus, there are two layers in a unit cell of a [110] nanowire and four and six layers in [100] and [111] nanowires, respectively. The governing equation for retarded Green's function G^R is

$$[E - H - e\phi(x) - \Sigma_S^R - \Sigma_S^R]G^R = I, \tag{1}$$

where Σ_S^R and Σ_D^R are contact self-energies and $\phi(x)$ is the electrostatic potential. The transmission function, which is equal to the number of conducting modes at a particular energy, and local DOS are given by

$$T(E) = \mathrm{tr}\{G^R\Gamma_S G^A \Gamma_D\}, \tag{2}$$

$$\mathrm{DOS}(E) = -\frac{1}{\pi}\Im m[G^R], \tag{3}$$

where $\Gamma_{S,D}=i[\Sigma_{S,D}^R-\Sigma_{S,D}^{R\dagger}]$ are the couplings between leads and the wire. The coupling of nanowires to metal leads is a complicated issue, requiring a systematic study. Experimentally, NWs usually make side contacts with metal leads, forming Schottky barriers. We choose to leave the discussion of the contact Schottky barriers beyond the scope of the paper, assuming that they can be regarded as additional contact resistances. In this paper, we focus on the intrinsic properties of NWs, assuming that contacts are made of ideal semi-infinite NWs. This ensures that all modes existing in ideal wire are coupled to the device. We assume that the electrostatic potential $\phi(x)$ changes linearly with the distance between source and drain. This is motivated by the fact that in the first approximation, surface roughness increases the resistance of the wire uniformly. We checked that a specific shape of potential profile does not change the current significantly. For most of the results of this paper, we use the Landauer-Büttiker expression to find ballistic current and a small bias conductance,

$$I_d = \frac{2e^2}{h}\int_{-\infty}^{\infty} T(E)(f_s - f_d)dE, \tag{4}$$

$$G = \frac{2e^2}{h}\int_{-\infty}^{\infty} T(E)(-\partial f_s/\partial E)dE, \tag{5}$$

where f_s and f_d are Fermi-Dirac distribution functions in the source and drain contacts.

We assume that NWs are n- or p-type conductors by setting chemical potentials of the contacts near the bottom of the conduction band or near the top of the valence band. The ability to change the type of conduction of NWs and nanotubes has been demonstrated experimentally by applying a back gate bias or introducing impurity doping.[3] In general, the Fermi energy of the wire at zero bias is determined by source and drain contacts, while the gate bias creates energetical shift of the band structure of the wire under the gate. Thus, by artificially changing Fermi energies in contacts with respect to the band structure, we are able to model the effect of gate bias in a transistor with a back gate contact controlling the entire length of the NW. By looking at the behavior of small bias conductance G as a function of contact Fermi energy E_F, one can get an insight to the behavior of transconductance $\partial I_d/\partial V_g$ of Si NW transistors.

In the last part of the paper, we include the effects of phase-breaking scattering. This is done by adding self-energies due to elastic and inelastic electron phonon scattering to Eq. (1) and solving an additional (Keldysh) equation for "less-than" Green's function $G^<(E)$. The details of the NEGF treatment of electron-phonon scattering are given elsewhere.[21]

III. RESULTS AND DISCUSSION

A. Transport in ideal NWs

The band structure of ideal nanowires is shown in Fig. 2, with the Fermi energies at zero bias plotted with the dashed line. The upper row shows the conduction band and thus is relevant to the transport in n-type nanowires. The lower row shows the valence band and is relevant to the transport in p-type NWs. As will be seen later, one of the main features of the band structure that affect ballistic electron transport in ideal NWs is the width of the conducting subbands, i.e., subbands crossing the Fermi energy. For example, the conducting subbands $c1$ in n-type and $v1$ in p-type [110] nanowire, shown in Fig. 2(a), have widths of around 1.3 V each. Similarly, the band structure of a p-type [111] NW shows that conducting subbands $v1$ have a width of more than 1 V. However, in n-type [111] NW, the conducting subband $c1$ has a width of only 350 meV and it is energetically separated

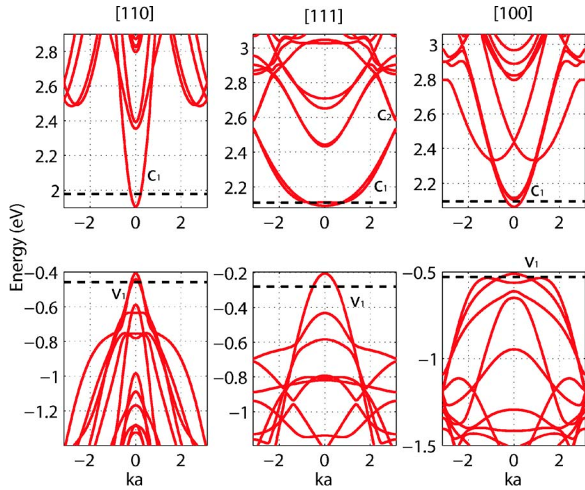

FIG. 2. (Color online) $sp^3d^5s^*$ tight-binding band structure of NWs shown in Fig. 1. The dashed line shows a position of the Fermi level in the wire at zero bias. The upper row corresponds to n-type and the lower row to the p-type wires. The widths of conducting subbands c_1 (n-type) and v_1 (p-type) determine the maximum bias under which the wire would conduct.

from the rest of the subbands. Finally, in n- and p-type [100] nanowires, conducting subbands have widths of around 800 meV, with a lot of subbands present in close energetical proximity.

The key features of the tight-binding band structure are reproduced within the more accurate DFT-GGA approach using VASP. Figure 3 displays the band structure of the [111] NW from the $sp^3d^5s^*$ tight-binding and DFT-GGA band structure. The most significant difference between the two band structures is the band-gap size due to well-known band-gap underestimation problem in DFT. This does not affect our transport results as we artificially set the NW Fermi level. Otherwise, the relative bandwidth and shape of the bands computed by the two methods agree very well.

The [111] wire conduction-band minima are composed of the six Δ valleys of bulk Si. In the effective-mass approximation, the energy minima of the [111] wire are located at $\pm 1/\sqrt{3}k_0$, where $k_0 \approx 0.85(2\pi/a)$ is the distance from Γ point to the conduction-band minima of bulk Si. The resulting band structure has a flat conduction band bottom and is almost a direct band gap. In the inset of Fig. 3, we zoom into the conduction band of [111] NW to compare the splitting observed at $ka=\pi$ and $E=2.56$ eV. Of the three lowest subbands, only two are degenerate, which is a consequence of noncircular cross section of the wire. The energy splitting which occurs at $ka=\pi$ is around 40 meV for the singlet and 70 meV for the doublet. DFT-GGA calculations show qualitatively the same band structure with the splittings equal to 20 and 50 meV, respectively, and a relative energy shift of around 30 meV. We also note that our calculations of the [100] band structure [Fig. 2(c)] are in agreement with previous studies.[11]

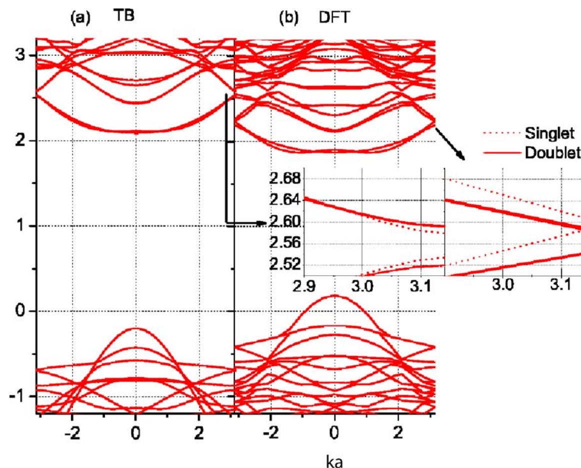

FIG. 3. (Color online) The (a) $sp^3d^5s^*$ tight-binding and (b) DFT-GGA band structure for the [111] NW. The splitting of subbands in n-type [111] NW at $ka=\pi$ is zoomed in.

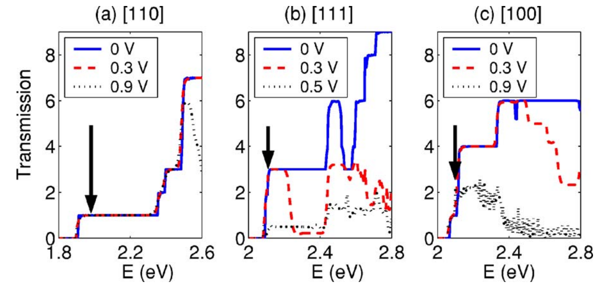

FIG. 4. (Color online) Transmission versus energy in ideal wires under applied drain bias V_d. Linear voltage drop is assumed. The arrows show the position of the Fermi energy E_{Fs} in the source contact, while the Fermi energy in the drain is $E_{Fd}=E_{Fs}-V_d$. (a) $T(E)$ in the transport energy window $[E_{Fd};E_{Fs}]$ is not changed by applied bias in n-type [110] NW. (b) In n-type [111] wire, $T(E)$ decreases at a bias higher that 350 mV. (c) In n-type [100] wire, transmission decreases dramatically when the bias exceeds 800 mV.

The width of the conducting subbands has important implications for transport properties: whenever the wire is biased above the conducting subband width, it will not conduct current because there is no energetical overlap between states in the source and drain. Electrons injected from the source will necessarily be reflected backwards if the DOS on the drain side vanishes. In order to characterize the electron conductance, in Fig. 4 we plot a transmission probability versus energy for different drain biases V_d. The transmission at zero bias shows a step at the bottom of the conduction band E_{cs} in the source contact. Because of the large width of the conducting subband in n-type [110] NW, the transmission in Fig. 4(a) is not changed significantly near source Fermi energy E_{Fs} when a bias is applied. However, one can see in Fig. 4(b) that for n-type [111] wire, the transmission near E_{Fs} decreases when the drain bias exceeds the subband width of 350 meV. Similarly, in n-type [100] NW, the transmission near source Fermi energy decreases as V_d exceeds 800 meV. We also note that when the drain bias exceeds the width of the conducting subband, the transmission does not vanish completely, as seen in Figs. 4(b) and 4(c). This is a consequence of a presence of other subbands. Under an applied bias, a symmetry of electron wave functions may be distorted. This can make a coupling between different subbands

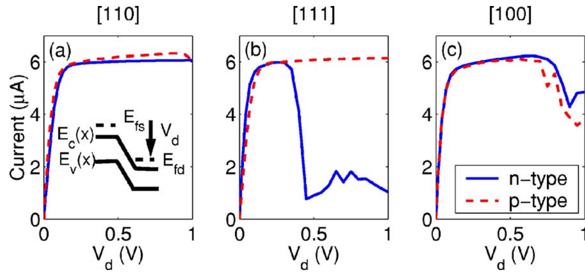

FIG. 5. (Color online) Drain current-drain voltage characteristics of ideal NWs shown in Fig. 1. The current falls off whenever bias exceeds the width of the conducting subband in Fig. 2. (a) both n- and p-type [110] NWs show perfect saturation of drain current, (b) In n-type [111] wire, the current shows a dramatic falloff when the drain bias exceeds 350 mV. (c) In n- and p-type [100] wires, the current falls off when the bias exceeds 800 mV. The current does not vanish completely due to intersubband coupling.

possible, which would open new channels of conductance and thus keep transmission and current nonzero. It is important to note that this intersubband coupling can also be caused by defects, surface roughness, or phonons.

In Fig. 5, we show current-voltage characteristics of ideal n- and p-type wires, whose cross sections are shown in Fig. 1 and band structure in Fig. 2. The length of all wires was taken to be around 100 nm. In accordance with Eq. (4), when a drain bias V_d is applied to an n-type wire, as shown in the inset of Fig. 5(a), the current flows, provided the transmission probability from left to right is nonzero in the transport energy window between Fermi energies E_{Fs} and E_{Fd} of source and drain. When the drain bias is small, current increases approximately as $(2e^2/h)V_dT(E_{Fs})$. The increase of the current occurs due to increasing number of electron states propagating from source to drain, which are not compensated by electrons propagating from drain to source. As drain Fermi energy E_{Fd} is pulled below the bottom of the conduction band in the source contact E_{cs}, the energy of uncompensated electrons injected from the source becomes limited from top and bottom by values of E_{Fs} and E_{cs}, respectively. These quantities are independent of bias, as they are the properties of source contact only. Therefore, at temperature $\mathbf{T}$, the current saturates at the value of $(2e^2/h)T(E_{Fs})k\mathbf{T}\ln\{1+\exp[(E_{Fs}-E_{cs})/k\mathbf{T}]\}$ or $(2e^2/h)T(E_{Fs})(E_{Fs}-E_{cs})$ when E_{Fs} lies in the conduction band. The analysis is similar for a p-type with the drain contact becoming the bottleneck for the current. The saturation value for a p-type wire is $(2e^2/h)T(E_{Fd})k\mathbf{T}\ln\{1+\exp[(E_{vd}-E_{Fd})/k\mathbf{T}]\}$ or $(2e^2/h)T(E_{Fd})(E_{vd}-E_{Fd})$ when E_{Fd} lies in the valence band.

Current-voltage characteristics of n- and p-type [110] NWs in Fig. 5(a) show a perfect saturation. As discussed above, the reason behind this is the large subband width and the weak dependence of transmission on bias. The transition from linear current increase to current saturation is also present in current-voltage characteristics of NWs in other growth directions. In these calculations, the Fermi energies in the contacts were chosen so as to yield the same value of saturation current of around 6 μA. The dependence of transmission on bias and ultimately the width of conducting sub-

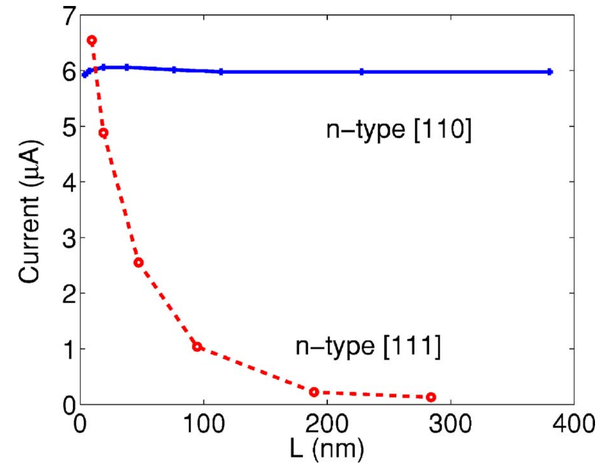

FIG. 6. (Color online) Saturation current at a drain bias of 1 V versus length of ideal [110] (solid) and [111] (dashed) NWs shown in Fig. 1. Energy splitting in the band structure of [111] nanowire causes a decrease of current in long nanowires. The onset of intersubband tunneling helps conduction and causes a recovery of current in short wires.

bands may significantly alter the current at high bias. This is seen as the dramatic falloff of current in Fig. 5(b) for n-type [111] NW, which occurs as drain bias exceeds the conducting subband width. The key reason for the current falloff is the subband splitting at $ka=\pi$ and $E=2.56$ eV, as shown in Fig. 3. We checked that this feature of the band structure is also present in nanowires with different cross sections. A similar but smaller in magnitude decrease of current is also observed in the case of [100] NWs. The negative differential resistance present in Figs. 5(b) and 5(c) may have important consequences for nanoelectronic applications involving Si nanowires.

The current in Figs. 5(b) and 5(c) does not vanish completely. As discussed above, the physics behind this effect is the intersubband coupling due to applied bias. An insight can be gained from Fig. 6, where we plot a value of the saturation current in n-type [110] and [111] nanowires under a bias of 1 V as a function of wire length. At this bias, [110] wire shows a saturation current of 6 μA for all wire lengths. The drain current in [111] wire is much smaller when the length of the wire exceeds 100 nm. As the wire length decreases, the electric field in the wire increases, which shrinks the width of energy barrier between lower and upper subbands. This is seen as the onset of the intersubband tunneling and recovering of saturation current.

B. Effect of surface roughness

We now discuss the effects of surface roughness on current carrying capacity of NWs. The surface roughness is introduced by adding, with probability 1/2, one monolayer at each facet in each unit cell of an ideal wire. The position of the bumps is completely uncorrelated and, therefore, this is a so-called "white noise" roughness. This model is motivated by the VLS fabrication method, in which vertical growth is assisted by a catalyst particle on the top end of the wire.

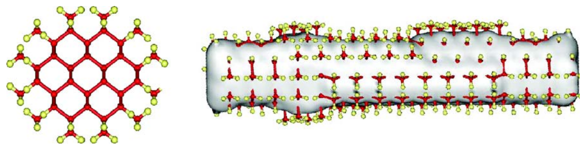

FIG. 7. (Color online) A cross section and a side view of 1.26-nm-thick [110] silicon nanowire with introduced "white noise" surface roughness and passivated with hydrogen. One atomic layer is added with probability 1/2 in each unit cell at each facet of the wire.

Fluctuations of the particle diameter in the liquid phase during the growth process lead to the variations of diameter of the NW from layer to layer. The resulting structure consists of a core with an ideal cross section and random "bumps" on the surface, as shown in Fig. 7.

Surface roughness results in fluctuating shape and area of wire cross section. Consequently, confinement of electrons vary along the axis. This is demonstrated in Fig. 8, where we plot a local DOS as a function of energy and coordinate. DOS was averaged over all atoms and all atomic orbitals in each atomic plane perpendicular to the wire axis. One can see that local DOS becomes nonhomogeneous in space and energy. In general, the conduction and valence subbands are shifted differently in each unit cell by a fluctuating confinement energy.

The irregularities of local DOS cause a reflection of electrons and a decrease of the transmission probability. In Fig. 9, we plot a small bias conductance $G(E_F)$ as a function of Fermi energy, computed using Eq. (5) for different growth directions in ~100-nm-long wires. For comparison, we also plot the conductance in ideal NWs. Ideal wire conductance takes integer values corresponding to the integer number of modes, passing through the wire. In the energy regions near the onset of new subbands, conductance shows a smooth behavior due to $k\mathbf{T}$ broadening. The conductance in rough

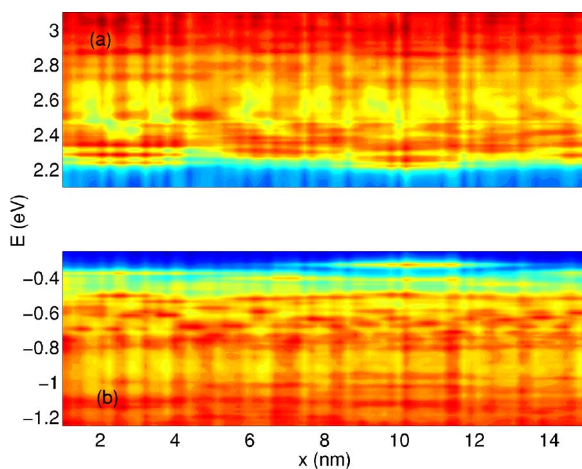

FIG. 8. (Color online) Logarithm of the density of states in (a) conduction and (b) valence bands as a function of energy and coordinate along the axis of the 1.26-nm-thick [110] wire with surface roughness. Density of states was summed over all atoms lying in a plane perpendicular to the axis. The spatial inhomogeneity of DOS causes reflection of electrons and decreases the current.

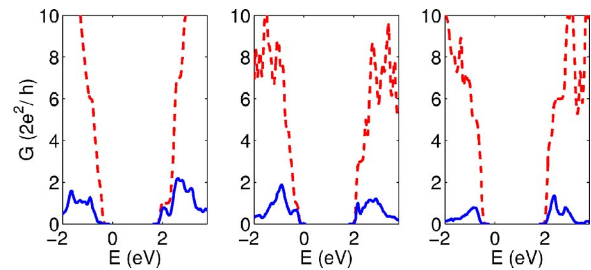

FIG. 9. (Color online) Zero bias conductance $G(E_F)$ versus Fermi energy in ~100 nm rough NWs, computed using Eq. (3). Conductance in rough NWs takes noninteger values and decreases in value. The decrease is more significant in the valence band, where the number of subbands increases more rapidly with energy. The effect of roughness is much stronger at high electron or hole energies due to a larger number of subbands and thus stronger intersubband mixing. Conductance shows local minima at energies corresponding to subband bottoms.

NW is smaller in magnitude and takes noninteger values, which indicates that electrons are reflected backwards. The strength of electron scattering due to surface roughness depends on the electron velocity $v=\partial E/\hbar\partial k$: slow electrons are reflected more easily by disorder causing a decrease in transmission and conductance.[15] Thus, the conductance shows dips near the energies corresponding to the onset of conducting subbands, where the velocity vanishes.

Another important factor in the suppression of conductance is a mixing of subbands induced by roughness. The effect of subband mixing is seen as the decrease of conductance with the increase of electron or hole energy. As the electron or hole energy increases, the number of subbands at this energy and the number of final states for scattering of electrons also increase.[14] Coupling between subbands randomizes electron motion by scattering electrons to oppositely traveling states or states with lower velocity, and thus decreasing total transmission and conductance through the wire. This has an important consequence for NW transistors: as the gate bias increases, the transconductance is suppressed. This factor may impose limitations on the maximum drive current one can achieve in NW transistors.

In Fig. 10, we plot the length dependence of drain current at applied drain bias of 1 V for different growth directions. Due to a random nature of roughness, we computed a current through an ensemble of ten NWs and took a mean value. In the case of [110] orientation in Fig. 10(a), surface roughness decreases current by 25% at $L\sim 100$ nm for n-type and by 83% for p-type NW. The keys to understanding the behavior of the length dependence of current are the electron velocity at the Fermi energy, the number of other subbands in the transport energy window, and electron velocity in those subbands. One can see that the slope of the conduction band is higher than that of the valence band in the vicinity of Fermi energies for n- and p-type wires. Thus, electrons in an n-type wire are less susceptible to reflections by the irregularities of the local DOS, which is the reason for a less steep dependence of current versus length in an n-type wire than that in a p-type wire.

Analogous to the case of the [110] wire, in the [100] wire [Fig. 10(c)], p-type conduction is, in general, more sensitive

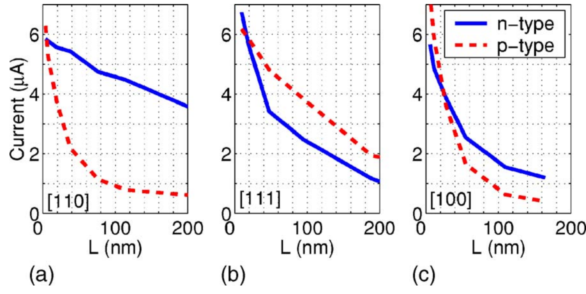

FIG. 10. (Color online) Saturation current at a drain bias of 1 V as a function of wire length for different growth directions. (a) The decrease of current in the [110] nanowire with length is more significant for the p-type case. (b) Current in the [111] wire shows similar trend to the [110] case, but the decrease of current is more significant. (c) Current in the [100] wire shows a dramatic decrease with length both for n- and p-type cases. One can see that 100 nm n- and p-type [100] NWs lose 85% of current.

to the surface roughness. This is also true for the [111] wire under a bias below 350 mV (not shown). At a bias of 1 V, the current in n-type [111], shown in solid line in Fig. 10(b), is lower than that in the p-type nanowire. This is caused by the energy splitting and current falloff, observed in ideal nanowire. It is interesting to note that the surface roughness actually increases the current in n-type [111] compared to the case of ideal wire in Fig. 6 by coupling subbands and opening new channels of conductance. Quantitative comparison of NWs with different growth directions shows that n- and p-type [100] and p-type [110] NWs are most sensitive to surface roughness, being only ~15% ballistic when the length is close to 100 nm.

As the diameter of the wire decreases, the ratio of surface to volume increases, and one would expect that the effects of the surface become stronger. However, Ref. 14 suggested that "surface roughness is less important in small-diameter Si NW transistors with few modes conducting than in planar metal-oxide-semiconductor field-effect transistors with many transverse modes occupied." The reason for this would be the reduced mixing of subbands. To check this prediction, we computed current in n-type [110] wire of smaller diameter of 0.46 nm with just one unit cell in the diameter direction. The Fermi energies were chosen to give a saturation value of current of 6μA at a bias of 1 V. At this bias, the number of subbands in the transport energy window decreased from 20 for the 1.26 nm wire to 4 for the 0.46 nm wire. In Fig. 11, we show a comparison of current in different diameter nanowires plotted in the log-log scale. The current shows a close to Ohmic ($\sim 1/L$) decrease in a technologically important range of small and moderate length ($L \leqslant 100$ nm) NWs. The decrease of current becomes much faster as the length increases and shows the exponential decay as one would expect in the regime of Anderson localization. If fitted to exponential function $\exp(-L/\zeta)$, the localization length ζ is close to 380 nm for 1.26 nm diameter wire. However, in smaller-diameter wire of 0.46 nm, surface roughness results in a much stronger decrease of current and a much shorter localization length of 12 nm. We thus conclude that the effects of surface roughness should be more pronounced in smaller-diameter nanowires.

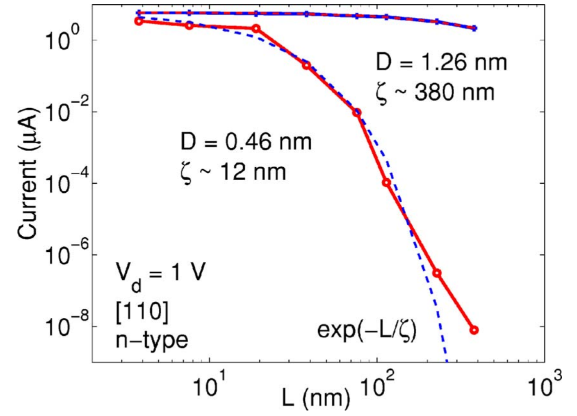

FIG. 11. (Color online) Saturation current of n-type [110] wires of 1.26 and 0.46 nm diameter at a bias of 1 V. The number of subbands in the transport energy window has decreased from 20 in the 1.26 nm wire to 4 in the 0.46 nm wire. When the wire length exceeds 100 nm, the current decreases exponentially with length as a manifestation of Anderson localization. Fitting with exponential function (dotted lines) gives an estimate of localization lengths of 380 nm for the 1.26 nm wire and 12 nm for the 0.46 nm wire.

Coherence of electrons is an important factor of electron transport in Anderson localization regime. A breaking of coherence due to electron-phonon scattering may reduce destructive interference and recover current in wires longer than the phase-breaking length. In order to see qualitatively how our results change in the presence of phase-breaking scattering, we include electron-phonon interaction within self-consistent Born approximation. Acoustic and optical phonons with $\hbar\omega = 62$ meV were taken into account. We estimate the deformation potential for electrons and holes by

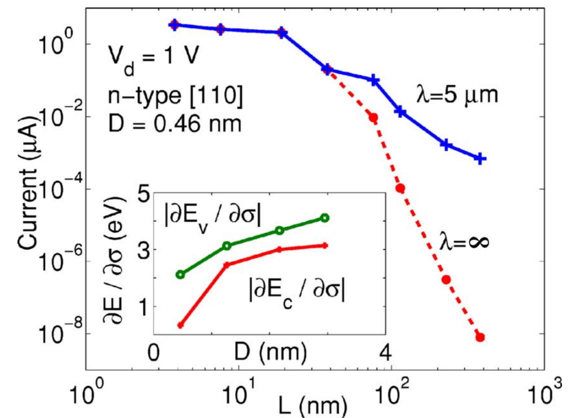

FIG. 12. (Color online) Saturation current of 0.46 nm [110] NW at 1 V in the presence of electron-phonon scattering (solid line) compared to the case of no scattering (dashed line). For wires shorter than the phase-breaking length $L_\phi \sim 40$ nm, electron-phonon scattering results in a slight decrease of current. In longer wires, the electron-phonon scattering causes an increase of current and recovering from Anderson localization regime. Inset: Deformation potential of [110] ideal NW as a function of diameter. The electron-phonon coupling strength in small-diameter nanowire is much smaller than in bulk Si. In the 0.46 nm wire, with Fermi velocity $v_F \sim 5 \times 10^5$ m/s, the mean free path λ_{ph} is estimated to be around 5 μm.

calculating the change of conduction and valence bands with a uniform tensile strain $|\partial E_{c,v}/\partial\sigma|$ using the same tight-binding scheme.[18] The deformation potential is found to be significantly lower in small-diameter wires than that in bulk Si, being only 0.5 eV for 0.46 nm wire and 2.5 eV for 1.26 nm wire. This results in a scattering rate of around 10^{11} s^{-1}. Figure 12 shows the length dependence of saturation current in 0.46 nm *n*-type [110] nanowire in the presence of electron-phonon scattering and compares it to that in the case without scattering. An equal deformation potential of 1 eV was chosen for both elastic and inelastic scattering. One can see that when the wire length exceeds a certain phase-breaking length $L_\phi \sim 40$ nm, the coherence of electrons is destroyed. As a result, current increases, recovering from Anderson localization regime. We note that, the phase-breaking length L_ϕ is much shorter than the mean free path λ_{ph}, which is estimated to be around 5 μm for electrons with Fermi velocity $v_F \sim 5\times10^5$ m/s. Thus, in Fig. 12 we can observe several regimes of electron transport, which occur due to interplay of surface roughness and phonon scattering: (i) $L < L_\phi$, the current shows exponential decrease $\sim\exp(-L/\zeta)$; (ii) $L > L_\phi$, the decrease of current becomes slower than exponential, but still not Ohmic ($\sim 1/L$). In a more technologically important case of wires with larger diameters and lengths below 100 nm, the phase-breaking length becomes shorter and the regime of Anderson localization is suppressed at shorter wire lengths. In this regime, when $L_\phi < L \sim \zeta < \lambda_{ph}$, one can still see the effects of surface roughness scattering as a faster than Ohmic decrease of current with length.

IV. CONCLUSION

In conclusion, we studied the effects of band structure and surface roughness on electron transport in small-diameter silicon NWs using tight-binding-NEGF approach. We showed that the band structure of ideal NWs may significantly affect current-voltage characteristics. Whenever drain bias exceeds the width of conducting subband, the current shows a dramatic falloff. This has important implications on nanoelectronic devices and circuits based on Si nanowires.

We find that surface roughness causes a significant decrease of current, which depends on the growth direction and conduction type. In wires thinner than 1 nm, surface roughness leads to a transition of electron transport from ballistic to Anderson localization regime. In a technologically important wire length range below 100 nm, the effects of surface roughness can still be observable as a faster than Ohmic decrease of current with length.

ACKNOWLEDGMENTS

We thank Intel Corporation for financial support and San Diego Supercomputer Center for providing computational resources. We are grateful to David Goldhaber-Gordon for helpful discussions.

*Present address: Silvaco International Inc., 4701 Patrick Henry Drive, Santa Clara, CA 95054. Electronic address: alexeis@silvaco.com

†Electronic address: pleu@stanford.edu

‡Present address: Departments of Physics and Electrical Engineering, University of Texas at Dallas, Richardson, TX 75083. Electronic address: kjcho@utdallas.edu

[1] D. D. D. Ma, C. S. Lee, F. C. K. Au, S. Y. Tong, and S. T. Lee, Science **299**, 1874 (2003).

[2] Y. Cui and C. M. Lieber, Science **291**, 851 (2001); X. F. Duan, Y. Huang, Y. Cui, J. F. Wang, and C. M. Lieber, Nature (London) **409**, 66 (2001); J. F. Wang, M. S. Gudiksen, X. F. Duan, Y. Cui, and C. M. Lieber, Science **293**, 1455 (2001); A. M. Morales, and C. M. Lieber, *ibid.* **279**, 208 (1998); Y. Cui, Q. Wei, H. Park, and C. M. Lieber, *ibid.* **293**, 1289 (2001); G. Zheng, F. Patolsky, Y. Cui, W. U. Wang, and C. M. Lieber, Nat. Biotechnol. **23**, 1294 (2005).

[3] Y. Cui, X. Duan, J. Hu, and C. M. Lieber, J. Phys. Chem. B **104**, 5213 (2000).

[4] M. S. Islam, S. Sharma, T. I. Kamins, and R. S. Williams, Appl. Phys. A: Mater. Sci. Process. **80**, 1133 (2005).

[5] M. Huang, S. S. Mao, H. Feich, H. Yan, Y. Wu, H. Kind, E. R. Weber, R. E. Russo, and P. Yang, Science **292**, 1897 (2001); S. S. Mao, R. E. Russo, and P. Yang, Proc. SPIE **4608**, 225 (2001).

[6] A. P. Alivisatos, Nat. Biotechnol. **22**, 47 (2004).

[7] T.-L. Chan, C. V. Ciobanu, F.-C. Chuang, N. Lu, C.-Z. Wang, and H.-M. Ho, Nano Lett. **6**, 277 (2006).

[8] F. M. Ross, J. Ross, and M. C. Reuter, Phys. Rev. Lett. **68**, 1 (2005).

[9] X. Y. Zhao, C. M. Wei, L. Yang, and M. Y. Chou, Phys. Rev. Lett. **92**, 236805 (2004).

[10] P. W. Leu, B. Shan, and K. Cho, Phys. Rev. B **73**, 195320 (2006).

[11] Y. Zheng, C. Rivas, R. Lake, K. Alam, T. B. Boykin, and G. Klimeck, IEEE Trans. Electron Devices **52**, 1097 (2005).

[12] Y-J. Ko, M. Shin, S. Lee, and K. W. Park, J. Appl. Phys. **89**, 374 (2001).

[13] A. K. Singh, V. Kumar, R. Note, and Y. Kawazoe, Nano Lett. **6**, 920 (2006).

[14] J. Wang, E. Polizzi, A. Ghosh, S. Datta, and M. Lundstrom, Appl. Phys. Lett. **87**, 043101 (2005).

[15] M. P. Anantram and T. R. Govindan, Phys. Rev. B **58**, 4882 (1998).

[16] C. Gómez-Navarro, P. J. De Pablo, J. Gómez-Herrero, B. Biel, F. J. Garcia-Vidal, A. Rubio, and F. Flores, Nat. Mater. **4**, 534 (2005).

[17] http://cms.mpi.univie.ac.at/vasp/.

[18] J. M. Jancu, R. Scholz, F. Beltram, and F. Bassani, Phys. Rev. B **57**, 6493 (1998).

[19] R. Lake, G. Klimeck, R. C. Bowen, and D. Jovanovic, J. Appl. Phys. **81**, 7845 (1997).

[20] A. Svizhenko, M. P. Anantram, T. R. Govindan, B. Biegel, and R. Venugopal, J. Appl. Phys. **91**, 2343 (2002).

[21] A. Svizhenko, and M. P. Anantram, Phys. Rev. B **72**, 085430 (2005).